Nat. Hazards Earth Syst. Sci. Discuss., doi:10.5194/nhess-2016-138, 2016
Manuscript under review for journal Nat. Hazards Earth Syst. Sci.
Published: 12 May 2016

Natural Hazards and Earth System Sciences
Open Access
Discussions

Factors controlling erosion-deposition phenomena related to lahars at Volcán de Colima, Mexico

Rosario Vázquez, Lucia Capra, Velio Coviello

Centro de Geociencias, UNAM, Blvd. Juriquilla No. 3001, 76230 Querétaro, México

Correspondence to: Rosario Vázquez (rvazmor@geociencias.unam.mx)

Abstract. One of the most common phenomenon at Volcán de Colima is the annual development of lahars that runs mainly through the southern ravines of the edifice. Since 2011 the study and the monitoring of these flows and of the associated rainfall has been achieved by means of an instrumented station located in Montegrande ravine, together with the systematic surveying of cross topographic profiles of the main channel. From these, we present the comparison of the morphological changes experimented by this ravine during the 2013, 2014, and 2015 rainy seasons. A total of 11 lahars occurred during this period of time, and their erosion/deposition effects were quantified by means of the cross-section areas determined from the profiles taken at the beginning and at the end of the rainy seasons and before and after the major lahar event of 11 June 2013. From the data compiled in these surveys, we identified two main zones: i) an erosive zone between 2100–1950 m a.s.l., 8° in slope, with progressive channel bed deepening and/or widening, and with an annual erosional rate of 10.3% due mainly to the narrowness of the channel and its high slope angle and, ii) an erosive-depositional zone, between 1900–1700 m a.s.l., (~8% erosion and ~16% deposition), due to a wider channel and that decreases in slope angle (4°). These observations were confirmed by simulating with the FLO-2D code a flow with a hydrograph similar to the 11 June 2013 lahar, the largest event observed during the investigated period. Based on these observations, the major factors controlling the erosion/deposition rates are the channel-bed slope, the cross section width and the joint effect of sediment availability and accumulated rainfall. On the distal reach of the ravine, the erosion or deposition processes tends to be promoted preferentially one over the other depending mostly upon the width of the active channel. Only for extraordinary rainfall events, lahars are mostly erosive all along the ravine up to the distal fan where deposition take place. Finally, by comparing rainfalls associated to lahars originated after the last main eruptive episode that occurred in 2004-2005, we observed that higher accumulated rainfalls were needed to trigger lahars in 2013 and 2014 seasons, which point to a progressive stabilization of the volcano slope during a post eruptive period. These results can be used as a tool to foresee the effects of future laharic events in Volcán de Colima and to improve the input parameters for the modelling of these flows, in order to better constrain the hazard zonation for lahars in this volcano.

1 Introduction

Lahars are concentrated mixtures of debris, sediment, and water that move rapidly down volcanic slopes under gravity (Smith and Fritz, 1989). According to their water-sediment rate, they can be defined as hyperconcentrated flows, between 20–60% by volume (Beverage and Culbertson, 1964), and extremely coarse sediment-rich debris flows with sediment concentration > 60% by volume (Costa, 1984, 1987; Pierson and Costa, 1987). However, as described by Pierson (2005), flow behavior will be strongly controlled by grain-size distribution, sediment-transport mechanisms, and their hydrodynamic characteristics. Flow volume and discharge can increase by several times downstream due to the entrainment of sediment and water (Vallance, 2000; Scott et al., 2005). Nonetheless, whether if it is a hyperconcentrated or a debris flow, or the evolution of both during the same event, the formation of lahars depends upon the availability of easily erodible sediments from the channel bed or lateral terraces, to bulk-up the flow (Scott, 1988; Pierson, 1995; Scott et al., 2005).

Nat. Hazards Earth Syst. Sci. Discuss., doi:10.5194/nhess-2016-138, 2016
Manuscript under review for journal Nat. Hazards Earth Syst. Sci.
Published: 12 May 2016

Also, additional volume changes can occur by dilution due to tributary streamflows, overrunning active stream channels or entrainment of water-saturated sediments (Pierson and Scott, 1985; Costa, 1987; Cronin et al., 1999). All of these flow changes are controlling the capacity of lahars to modify the morphology of the channels were they flow, as observed in several studies (Muñoz-Salinas et al., 2008, 2009; Doyle et al., 2011; Starheim et al., 2013; Andrés de Pablo et al., 2014), not only in volcanic environments, but also in mountainous regions in the form of debris flows, where the role that play the slope, the sediment availability, rainfall distribution and flow dynamics, among other parameters, has been long studied in these environments (e.g. Coe et al., 2008; Guthrie et al., 2010; Berger et al., 2011; Abancó and Hürlimann, 2014; Theule et al., 2015), and has served to extrapolate these findings to the volcanic conditions.

Previous studies found that the highest erosion rates in river basins (10^5-10^6 $m^3km^{-2}yr^{-1}$) correspond to active volcanoes under humid climate (Milliman and Syvitski, 1992; Walling and Webb, 1996; Major et al., 2000). As observed by Lavigne (2004), on these types of volcanoes, the efficiency of erosion is a consequence of rain-triggered lahars that develops during the rainy season, converting the estimation of sediment yield and erosion rate a very difficult task to achieve (Lavigne, 2004; Procter et al., 2010; Pierson et al., 2011; Thouret et al., 2014). However, several studies have been realized in order to analyze the erosional and depositional processes of active channels on volcanic environments along with the factors that controls them (Major et al., 2000; Lavigne, 2004; Berger et al., 2011; Pierson et al., 2011; Starheim et al., 2013; Thouret et al., 2014). Based on these studies, main factors affecting erosion and depositional rates are: the amount of rainfalls and volume of sediments available, the hydrologic characteristics of the stream-bottom deposits, flow depth, bed-slope gradient and the morphology of the channel (Mizuyama and Kobashi, 1996; Fagents and Baloga, 2006; Berger et al., 2011; Okano et al., 2012; Thouret et al., 2014). Moreover, a number of studies address the issue of identifying governing factors of debris flow entrainment and most of them have been carried out in laboratory (Mangeney et al., 2010; Iverson et al., 2011) or in mountain environments (e.g. Chen et al. 2005; Hungr et al. 2005; Guthrie et al., 2010; Berger et al., 2011; McCoy et al., 2012; Abancó and Hürlimann, 2014; Theule et al. 2015). These latter studies show large scattered results, which suggests that mechanisms governing the entrainment are complex and depend from site and flow characteristics. However, sediment availability and channel shape appear to be the most important parameters governing debris flow entrainment.

At Volcán de Colima, one of the most active volcanoes in México, the annual occurrence of lahars during the rainy season is a common feature that has allowed to study the development and dynamics of these flows. Since 2011, the formation and evolution of lahars were monitored along the Montegrande ravine, a gorge located in the southern slope of the volcano, and one of the most actives in laharic activity. The real-time monitoring of these phenomena has been conducted by means of a monitoring station located at 2000 m a.s.l. (for a detailed description of the equipment see Vázquez et al., 2014, 2016), along with topographic profiles and field data obtained during the 2013–2014 seasons. From these data, it was possible to analyse and describe the annual sediment and erosion balance on selected sites, and the factors that mostly control the erosion-deposition processes. No important volcanic activity producing pyroclastic flow deposits on the volcano slope was reported for this period, fact that could have altered the annual sedimentation rate. The results presented here can contribute to better define lahars mitigation strategies and hazard assessment, and to determine the most suitable sites for lahar monitoring and better understand lahars behavior at Volcán de Colima.

2 Morphological features of Montegrande ravine

Volcán de Colima is an almost perfect cone-shaped stratovolcano, and has a slope that varies between 40°–35° from the summit at 3840 m a.s.l., and decreases to < 10° towards its base (Capra et al., 2010) at ~ 1600 m a.s.l. (Fig. 1). The ravines where lahars develop annually are located in the southeastern and southwestern sector of the edifice. In this paper we will focus on Montegrande ravine which is one of the most actives ravines in forming lahars (Fig. 1), and has been being monitored since 2011 (Vázquez et al., 2014, 2016).

Nat. Hazards Earth Syst. Sci. Discuss., doi:10.5194/nhess-2016-138, 2016
Manuscript under review for journal Nat. Hazards Earth Syst. Sci.
Published: 12 May 2016

Natural Hazards and Earth System Sciences
Open Access
Discussions

The Montegrande ravine begins where two main gullies connect at the main break in slope of the cone (from 30 to ~20°), at approximately 2400 m a.s.l. (e.g. the proximal zone, Fig. 1-I a, b, and II); after this, the ravine extents for ~6.5 km long, comprising the intermediate zone, from ~2300 to 1900 m a.s.l., where the slope decreases to ~8° (Fig. 1-I c, d, e, f, and II), and the distal zone located from 1900 to 1600 m a.s.l. at the mouth of the ravine, where the main channel opens to a wide fan where the slope decreases to ~2° (Fig. 1-I g, h, and II) and lahars discharge all their loads (Fig. 1h). The ravine formed by the erosion of Holocene debris avalanche deposits, and pyroclastic flow deposits (PFD) from the 1913 plinian eruption, with vertical walls up to 20 m in height and up to 70 m in width (e.g. Fig. 1a and b). The active channel is highly variable in width, from 20 m to very narrow sections of ~3 m (Fig. 1c, d, e, f, and g) and is flanked by few meter-high of historic laharic terraces (e.g. Fig. 1c). In addition, the ravine presents a complex morphology downwards, showing in some places straight paths, and in others tight turns of around 60°–20° (Fig. 1-I). Where the ravine ends, the power lines of Comisión Federal de Electricidad (CFE), the National Power Company, crosses the entire width of the fan (Fig. 1-I), and because of this, during the lahar season they are prone to be damaged, as occurred in previous years (Davila et al., 2007).

The Montegrande ravine is an ephemeral stream channel. When the rainy season begins (in June for this region, Davila et al., 2007; Capra et al., 2010), and lahars start to flow down, the morphology of the main channel and the terraces that flanks it evolves markedly (Figs. 2a and b). Meanwhile, during the dry season, the main channel is filled up by wood debris and small failures from the banks (Fig. 2c).

3 Methodology

The study of the morphological changes suffered by Montegrande ravine during the 2013-2015 seasons associated to the laharic activity was carried out by taking topographic profiles perpendicular to the flow path in selected sites (e.g. Fig. 2d) and by monitoring rainfall trends in the basin. Five checkpoints were selected and their respective topographic profiles were taken on 11 and 12 June, 30 July, and 11 October of 2013, on 12 September 2014, and on 18 March 2015. These sites are numbered from MG_01 to MG_05, starting from the monitoring site at ~2000 m a.s.l. within the intermediate zone (Fig. 1-I c, and II), up to the mouth of the ravine in the distal zone (Fig. 1-I). In addition, we also take into account two profiles within the portion of the monitoring site named MG_T-P1 and MG_T-P2. All profiles were taken and are presented here, looking upflow (i.e. towards the volcano crater, Fig. 2d).

For the topographic surveys, we used a laser distance-meter and for each site, reference pictures and GPS points were taken (e.g. Fig. 2d). We also leave marks on trees, walls or big clasts (>1.5 m in diameter) (Fig. 2d), in order to easily identify the sites during the field campaigns, and to use them as control marks for comparing the topographic profiles between each campaign. A HOBO RG3 water station with a rain gauge sensor of 0.2 mm resolution, and sampling within one minute intervals (Capra et al., 2010; Vázquez et al., 2016), installed at the monitoring site (Fig. 1-I c, and II), was used to monitor the rainfall events that triggered the lahars at Montegrande ravine.

Morphological changes are here compared based on the results of topographic surveys. We analyze and classify the flows that occurred during the 2013-2015 seasons (Table I) following the methodology described in Vázquez et al. (2016), which is based on monitoring data gathered at Montegrande monitoring site and identifies single-pulse events (SPE), and multi-pulse events (MPE). The SPEs are characterized by a flow that lasts 1-1.5 hrs and develops a single-front enriched in blocks (FEB), followed by diluted surges (DSs); whereas the MPEs present more than one FEB interspersed by a sustained flow showing changes in flow discharges (DSs) and lasts up to 3 hrs, ending with a prolonged streamflow.

Only for the 11 June 2013 lahar, topographic surveys were performed the day before and after the event. In the other cases, profiles are mostly taking into account the annual season of lahars (Table I). For example, between

Nat. Hazards Earth Syst. Sci. Discuss., doi:10.5194/nhess-2016-138, 2016
Manuscript under review for journal Nat. Hazards Earth Syst. Sci.
Published: 12 May 2016

Natural Hazards and Earth System Sciences
Open Access
Discussions

the field campaign of 30 July 2013, two lahars formed; after this and until the next field campaign on 11 October, just one lahar took place (see Table I). During the 2014 season, 7 lahars developed until the field campaign on 12 September; and between these surveys and the survey taken on 18 March 2015, the only lahar developed was on 17 March 2015 (Table I). Thus, the morphological changes described in the following sections are related to the beginning and at the end of these seasons.

To quantify the erosion/deposition rates, for each section, a discrete areal value was computed and used to calculate it (e.g. Fig. 3a and b), after a SPE (such as the 11 June 2013, Figs. 3c, d, and 4) and seasonally (Fig. 5), in order to estimate the 2013 and 2014 annual balances (e.g. Fig. 6). For each checkpoint, the topographic profiles are superimposed to observe qualitatively channel variation in depth and width during the 2013-2015 seasons (Fig. 5). To do so, the topographic profiles were embedded in a rectangle of a known area (Fig. 3a and b), and the rates *E* (erosion) and *D* (deposition), were determined according to the following statements (Fig. 3a and b):

1) During Date t_1, and Date t_2, for the same site: x = x' and y = y', hence:
$$A_T = x * y = 100\ \%$$
2) During Date t_1, $A_1+A_2 = A_T = 100$ %; also, during Date t_2, $A_3+A_4 = A_T$, hence:
$$A_1+A_2 = A_3+ A_4 = 100\ \%$$
3) There will be erosion (*E*), if between Date t_1 and Date t_2, $A_3 > A_1$ and $A_4 < A_2$
4) There will be deposition (*D*), if between Date t_1 and Date t_2, $A_3 < A_1$ and $A_4 > A_2$

From these remarks, the areal values A_T, A_1, A_2, A_3 and A_4, along with the rates *E* and *D*, were estimated for the dates reported in the table of Fig. 7.

4 Results

4.1 Morphology of Montegrande ravine before and after the 11 June 2013 lahar

The systematic surveying of the topographic profiles over the checkpoints in Montegrande, started in 2013, after the 11 June 2013 lahar, described and classified by Vázquez et al. (2016) as a MPE (Table I). It was the first lahar of the 2013 season, and has been one of the biggest events recorded in the ravine since 2011. It consisted of a flow that lasted approximately 3 hours, and presented several FEBs, followed by DSs. The total rainfall associated to this lahar was 117 mm accumulated in ~3.5 hrs with a maximum peak intensity of 131 mm/hr (Table I). For this lahar, we took profiles the day before and the day after (Figs. 3c, d, and 4) the event, which allowed us to outline quantitatively the *E* and *D* rates (Fig. 7f), and served as an example of the effects of a MPE under extreme hydrometeorological conditions.

In general, the MPE of 11 June 2013 eroded the channel bed of the ravine by 1 m deep in average, as could be observed in Fig. 3d, and from the profiles of checkpoints MG_01, MG_02, and MG_03 (Figs. 4a, b, and c, respectively). However, from the profiles of MG_04, and MG_05 sites (Figs. 4d and e), is clear that both erosion and deposition processes were acting simultaneously. In fact, on checkpoint MG_05, the lahar left a final deposit that filled up the channel bed by 1 m, at least, but eroded the right later terrace. In general, along the ravine, erosion was predominant in the channel bed, than in the walls; however in some portions of the ravine, the erosion tends to wash away preferentially one side of the channel than the other, developing a lateral migration of the channel axis (e.g. Fig. 4a and c).

The width of the active channel also varied after the 11 June 2013 lahar, becoming ~2 m wider especially on MG_01 and MG_02 sites (Figs. 4a and b), but to a lesser extent (<1 m) in the other sites (Figs. 4c, d, and e).

4.2 Morphological evolution of Montegrande ravine within the 2013-2015 field campaigns

Nat. Hazards Earth Syst. Sci. Discuss., doi:10.5194/nhess-2016-138, 2016
Manuscript under review for journal Nat. Hazards Earth Syst. Sci.
Published: 12 May 2016

Besides the MPE of 11 June 2013, three more lahars were developed during the 2013 rainy season (Table I), for which additional observations are here provided for that year. In 2014, more than 5 flows were observed, classified and analyzed, and the annual balance is here presented based on a survey before and after the season. Finally, for 2015 only data gathered after the first lahar of the season is here described (Figs. 5, 6, and Table I).

Figure 5 shows the profiles of the channel bed of Montegrande ravine, from the monitoring site (at ~2050 m a.s.l., Fig. 5a), towards the mouth of the ravine (at ~1750 m a.s.l., Fig. 5g). In all profiles, the same color corresponds with the same year, and the gradient of its color corresponds to different field campaigns. The segmented lines represent erosion-dominated respect to the previous profile, while the continuous lines represent deposition-dominated (Fig. 5).

The first checkpoint (MG_T-P1) is located within the channel section that is being monitored by the videocamera (e.g. Figs. 1c, 3c, and 3d). In this site, the channel morphology doesn't change significantly through the seasons. Little variations of the channel axis position are observed, which tends to migrate to the left side of the bank, towards the wall of an old terrace (Fig. 5a). After the event that occurred on 17 March 2015 the channel becomes narrower (from ~14 m to ~12 m) due to a new small terrace development along the left bank, and to a small collapse of the right wall occurred during the dry season (Fig. 5a).

Checkpoint MG_T-P2 (Figs. 1-I and 5b), situated ~20 m downstream from MG_T-P1, shows an increase in depth of the channel from June to July 2013, from ~1.5 m to ~5 m (Fig. 5b). For this checkpoint, we only took the topographic profiles during the 2013 season since in 2014 the exact location of this site was not recognizable.

The MG_01 checkpoint is located ~80 m downstream from the monitoring site (Fig. 1-I), shows a progressive increase in depth, by almost 2 m (Fig. 5c) and becomes narrower from 7 m wide at the beginning of the 2013 season, to ~2 m wide at the end of the season. It is also evident that the terraces that flank the active channel were eroded by more than 2 m depth (Fig. 5c) during the 2013- 2014 seasons.

The next checkpoint (MG_02, Fig. 5d) is located approximately 750 m downstream from the MG_01 site (Fig. 1-I), where the channel path is almost rectilinear and has a regular width of ~10 m. As could be observed from the overlapping of the profiles (Fig. 5d), the process of erosion dominates at this site, deepening the channel bed almost 4 m, and extending its width up to 15 m, but conserving the main axis at the same place (Fig. 5d).

The following checkpoint MG_03 (Fig. 5e), situated 300 m downstream from the previous one (Fig. 1-I), marks the beginning of an almost straight path of ~1,200 m downwards, where the ravine widens from ~15 m to >30 m, and their vegetated walls become steeper (>30 m height). Here the profiles (Fig. 5e) present alternation of erosion and deposition processes within a narrow active channel of ~12 m width. The erosion dominated up to 30 July 2013; but at the end of the 2013 season the channel became wider and was filled up with more than 2 m of sediment. By September 2014 a new terrace was formed on the right side of the channel, narrowing its previous width (~12 m) by ~2.8 m, and was deeply eroded by the 17 March 2015 lahar, showing a tendency to recover its initial morphology (i.e. that from 11 June 2013, Fig. 5e) but moving the channel axis to the left side.

The MG_04 checkpoint is located at approximately 800 m downstream from the MG_03 site, just before the path of the ravine makes a turn into another straight segment (Fig. 1-I). At this site, the changing morphology of the channel is due again to a combination of erosion/deposition processes (Fig. 5f). After the 11 June 2013 lahar, the channel was progressively filled up mostly by the accretion of the lateral terraces that narrowed the channel, from ~10 m to ~7 m. After 30 July 2013 these newly formed terraces were eroded by the end of the 2013 season resulting in a 15-m wide channel (Fig. 5f). During 2014, depositional processes dominated by filling the channel which main axis migrated to the right, to recover in 2015 a morphology similar to the main channel shape at the beginning of the 2013 season. (i.e., 11 June 2013, Fig. 5f).

Nat. Hazards Earth Syst. Sci. Discuss., doi:10.5194/nhess-2016-138, 2016
Manuscript under review for journal Nat. Hazards Earth Syst. Sci.
Published: 12 May 2016

Natural Hazards and Earth System Sciences
Open Access
Discussions

The morphology of the last checkpoint (MG_05), located ~650 m downwards (Fig. 1-I), is also the result of a combination of erosion and deposition processes. Similarly to checkpoints MG_03 and MG_04, the morphology of the channel tends to be recovered (Fig. 5g) but with a lateral migration of the main axis towards the left side through the season. After the 11 June 2013 lahar, the active channel continues to be filled up by the successive flows (Fig. 5g), decreasing its depth of about 2 m, as observed by the 30 July campaign. By 11 October 2013, the channel suffered a major morphological change, widening from ~7 m to ~18 m, and deepening the channel bed 1 m in the central axis (Fig. 5g). During the 2014 season and from the evidences of the 18 March 2015 campaign, it could be observed that the lateral terraces were built up again, and the morphology of the middle portion of the channel tends to be recovered (Fig. 5g).

Based on the morphological changes here described, and based on the characteristics of lahar events recognized during the 2013-2015 period and on the associated rainfalls that triggered them, the 11 June 2013 lahar can be classified as an extraordinary event (Fig. 8), predominantly erosive at all checkpoints, while subsequent lahars during the 2013 season had a variable behavior. During 2014 depositional process dominated, and the 17 march 2015 lahar had a variable behavior (Fig. 5).

4.3 Annual erosion/deposition balance in Montegrande ravine

4.3.1 The 2013 season

During 2013, four lahars were detected on the Montegrande ravine (three MPE and one SPE), and their hydrological characteristics are listed in Table I. Total rainfall in Montegrande during 2013 was up to 580 mm, and the 11 June event corresponds with an exceptional accumulated rainfall of 117 mm (Fig. 8).

At checkpoints MG_01 and MG_02 erosion processes dominate with ~12% of erosion on average of the channel bed (Figs. 6a, b, and 7f), mainly on the main axis of the channel, At the end of the 2013 season, the depth of the channel at checkpoint MG_01 was 2 m deeper than at the beginning (Fig. 5c and 6a), and the channel width become wider, from ~7 m to ~15 m (Fig. 5c and 6a). On checkpoint MG_02 (Fig. 6b), the level of erosion was lower, deepening the channel bed ~2.5 m and widening it up to 6 m at the end of the season (Figs 5d and 6b).

In the subsequent checkpoints (MG_03 to MG_05, i.e. Figs. 6c, d, and e) located down flow the ravine, the rate of erosion–deposition phenomena was more-less balanced (Fig. 7f). On checkpoint MG_03 (Fig. 6c), at the end of the 2013 the cannel was filled by up by 2 m-thick of sediments reaching a 11 m-width by the erosion on lateral walls.

On MG_04 checkpoint the rate of deposition was larger according to the values on the table of Fig. 7f, even when as could be seen in Fig. 6d, erosion and deposition are present within the profiles. The main change in the morphology of the site was the widening of the channel, from ~10 m (on 11 June, Figs. 5f and 6d) to ~13 m at the ending of the season, but with an accretion of the channel bed of up to 2 m. It is worth to observe that the widening of this part of the channel was preferentially towards the right bank of the bed axis (Fig. 6d).

Finally, on checkpoint MG_05 (Fig. 6e), the level of erosion during 2013 season was more evident with a value of ~8% that correspond with the widening of the channel from ~8 m to ~16 m (Fig. 6e), but with a deposit in the middle axe of ~ 0.5 m in thickness by the end of the season.

4.3.2 The 2014 season

During the 2014 season the total rainfall in Montegrande ravine was of ~540 mm. In comparison with the 2013 season, the changes in the morphology of the checkpoints were dominated rather by the process of deposition, than by erosion (Fig. 6), even when 7 lahars were developed during 2014 (five MPE and two SPE, Table I).

Nat. Hazards Earth Syst. Sci. Discuss., doi:10.5194/nhess-2016-138, 2016
Manuscript under review for journal Nat. Hazards Earth Syst. Sci.
Published: 12 May 2016

In general, at checkpoints MG_01 and MG_02 (Fig. 6f and g), the rate of erosion was higher than in the down flow checkpoints (MG_03, MG_04, and MG_05, Figs. 6h, i, and j, respectively), but not that high in comparison to the 2013 season (Figs. 6a to e, and 7f).

On checkpoint MG_01 (Fig. 6f), the erosion was mainly focused on the walls of the terraces that flanks the channel axis, eroding ~8 % of the material, diminishing its height by 2 m, but conserving the active channel width in ~2.5 m with a final deposit of ~1 m in thickness (Fig. 6f). On the other hand, at checkpoint MG_02, both erosion/deposition are present, (Fig. 6g), with a final deposition rate of 0.7% (Fig. 7f) and conserving the main morphology through the season, i.e. a wide channel (~16 m width), flanked by terraces of 5 m height (Fig. 6g).

Contrary to the observed balance on *E-D* rates for the MG_01 and MG_02 sites, on the successive checkpoints the deposition process dominates. For instance, at site MG_03 (Fig. 6h) the channel width reduced from ~11 m to ~8 m, due to 18.5 % of deposition within the channel bed forming a new terrace on the right side of the channel. Similarly, at checkpoint MG_04 (Fig. 6i), the width of the channel reduced from ~16 m to ~5 m, because of the ~20 % of deposition (Fig. 7f) left in the channel bed, with the formation of new terraces along the flank of the active channel (Fig. 6i). Finally, at checkpoint MG_05 (Fig. 6j), a morphology similar to the MG_03 site can be observed, where new material deposited preferentially on the right side of the channel wall (D = 9.6%), leaving vertical steps and narrowing the channel from ~16 m to ~14 m (Fig. 6j).

5 Discussion

Based on the analysis of the cross-section profiles within the checkpoints MG_01 to MG_05 (e.g. Figs. 5 and 6) taken during 2013, 2014, 2015 seasons, the rainfall features that triggered them (Fig. 8) and the number and type of lahars occurred during the surveyed period, it was possible to analyze the main factors in controlling the evolution of the Montegrande ravine. Field evidences point that erosive processes dominate in the intermediate zone (i.e. checkpoint MG_01 and 02), where slope gradient is up to 8°, respect to the more distal sites where both erosion and deposition acts because the ravine becomes wider and the slope diminishes from ~6° to 4°, i.e. checkpoints MG_03 to MG_05 (Fig. 1). This behavior is in agreement with the hydrogeomorphological model proposed by Lavigne (2001), that identifies the chief process that shape the channel morphology in three main channel segments: (1) a proximal segment where riverbed and bank erosion is continuous (i.e. from MG_01 to MG_02); (2) an unsteady transitional zone, where erosional processes alternate with depositional processes (i.e. from MG_03 to MG_05); and (3) a distal segment where sediment deposition is continuous (in this case, the alluvial fan of Montegrande ravine).

The 11 June 2013 lahar represents an exceptional event that was erosive almost all along the ravine. This lahar was associated with an extraordinary rainfall event (117 mm of accumulated rain, Table I) that developed a large and highly erosive flow. Similar exceptional events have been previously observed in the same ravine during the Jova hurricane, which also developed a high-magnitude lahar that deeply eroded the channel (Capra et al., 2013).

In order to better constrain the influence of the channel morphology on the observed erosion/deposition rates, simulations with FLO-2D code were performed (O'Brien et al., 1993). The program routes floods over natural channels solving the full-dynamic wave equation. It has a utility for sediment-transport that can compute sediment scour and deposition. Here the sediment transport capacity equation of Zeller-Fullerton was used (Zeller and Fullerton, 1983; Yang, 1996), (e.g. Fig. 7). For the inflow, the hydrograph of a MPE-type similar to the 11 June 2013 lahar estimated from the seismic record was used (Vazquez et al., 2016), with two maximum peak discharges of 60 m^3/s and 26 m^3/s along 4 hours of flooding. The scope of the simulation is to observe if by simulating clear water, the morphological changes along the channel are similar to those observed by field survey. Similar rates will point to a main control of the channel morphology on sediment transport. This only

Nat. Hazards Earth Syst. Sci. Discuss., doi:10.5194/nhess-2016-138, 2016
Manuscript under review for journal Nat. Hazards Earth Syst. Sci.
Published: 12 May 2016

pretend to be a qualitative comparison, since absolute depositional rates cannot be compared with those observed on the field. In fact, lahars observed at Volcán de Colima have sediment concentration between 30% and 50%, from hyperconcentrated to debris flow (Vázquez et al., 2014) and depositional rates within these types of flow are higher respect to a flow free of sediment-load (Costa, 1987). The same happens for the erosion, since clear water can be more efficient in eroding the river channel, but lahars commonly induce the collapse of lateral embankments or the entrainment of large blocks from the flow front (Fagents and Baloga, 2006). Despite this assumption, values obtained from the simulation are quite in agreement with those observed in the field (Fig. 7f). In particular, section MG_01 and MG_02 are dominated by erosion (Figs. 7a, and b), mostly deepening the channel, and from MG_03 to MG_05 depositional processes dominates (Figs. 7c, d, and e). The simulation outcome of the 11 June 2013 lahar still presents discrepancy with the results of the field survey but, since as previously stated, it was an extraordinary event. Based on these results, the slope represents the first major factor in controlling *E-D* rates, as changing from 8° to 5°, depositional processes seems to dominate over erosion (Fig. 7c, d, and e). For example, the ravine morphology at sections MG_01 and MG_04 is quite similar, with a ~80 m-long straight channel, bracketed by two narrow bends, but at MG_04 section, with ~5º in slope, depositional processes are dominating. Depositional process at Montegrande ravine dominate where the channel-bed slope is smaller than 5°, which represents a higher value than that observed in Ruapehu of ~2.7–0.7° (Fagents and Baloga, 2006) or the <1.2° found by Pierson (1995) for snow-clad volcanoes; but similar to the values observed in Popocatépetl volcano (i.e. <6.5°, Capra et al., 2004; Muñoz-Salinas et al., 2008, 2009). Furthermore, the dominant erosional behavior of lahars that has been observed in Montegrande ravine where channel slope settles above 8° is consistent with the observation made in Alpine basins affected by debris flows (e.g., Theule et al., 2015).

The second parameter that affects erosion and depositional process at Montegrande ravine is the cross section width. As stated before, at distal sections (MG-04 and MG-5) erosion and deposition processes alternate and this behavior appears to be controlled by the channel width variation. The erosion dominates as the channel reach a critical width after which deposit starts forming new terraces along the channel wall (Figs. 5f and g). As the channel narrows again, erosion take place. Changing in channel width clearly controls flow discharge, so a narrow channel promote erosion but as it became wider it induce deposition. These same behaviors and factors controlling the morphological changes, have been reported in other volcanoes as well (e.g. Mount Ruapehu, New Zealand, Procter et al., 2010). Moreover, this is in agreement with the observations made by Abancó and Hürlimann (2014) in Alpine catchments affected by debris flows, where channel-bed slope, cross-section shape and sediment availability (see the following) have been identified as the most relevant factors controlling the erosion process.

The joint-effect of two others parameter acting together, i.e. the accumulated rainfall and the sediment availability, is the last fundamental factor that governs erosion and depositional processes at Montegrande ravine. At Volcán de Colima, even a very low rainfall as observed in previous years can trigger lahars (Capra et al., 2010, Fig. 8), but the resulted flows are low in magnitude and, as directly observed, they induce progressive sediment accretion forming new lateral terraces on the channel (Figs. 2 and 5). However, as observed in recent years, long-lasting rainfall events are needed to trigger a lahar (Fig. 8). This has important implications, since after a main eruption, lahar frequency increase due to the immediate reworking of pyroclastic material (Manville et al., 2009), but their magnitude will depend on the rainfall characteristics and the volcaniclastic material available, until it progressively decreases in the following years, as observed at Volcán de Colima (Davila et al., 2007; Capra et al., 2010) and other volcanoes (Lavigne, 2004; Thouret et al., 2014). These factors, along with the physical features built up by the flows (i.e., sediment load, depth, volume, discharge, etc.) will control the morphological evolution of the ravine, until the landscape response to the volcanic perturbation returns to background conditions (Manville et al., 2009; Thouret et al., 2014). This dynamics is evident in Montegrande ravine, where the sediment availability has been decreasing in the last years. The eruptive phase occurred in 2004-2005 is the last significant phase of sediment supply that occurred

along the volcano flanks. Block-and-ash flows (BAFs) emplaced on main ravines up to 6.5 km from the crater (Macías et al., 2006; Sulpizio et al., 2010), due to the repetitive growing and collapse of the summit dome (Fig. 9a). Then, a new period of slowly dome growing begin in 2007 and stopped in 2012, after reaching the crater rim and spilling over on 2011 (Capra et al., 2015; Fig. 9b). Finally, a phase of low activity characterized the 2013-2014 years (Fig. 9c). Consequently, a period of approximately five years (during the intra-eruptive period, from 2007 to July 2015, Capra et al., 2016), was needed to recover the hydrological and sedimentary-yield balance to background conditions. This dynamics is in agreement with the recovering times observed after minor eruptions (Manville et al., 2009).

6 Conclusion

The systematic monitoring of the morphological changes observed in Montegrande ravine in the past years, served as a starting point for the analysis of the geomorphic modifications due to post-eruptive lahars in an active channel in a volcanic environment.

Channel-bed slope, cross-section width and the joint effect of sediment availability and rainfall magnitude are the main factors controlling erosion/depositional processes at Montegrande ravine. In particular, the proximal and middle reaches, where bed load is up to 10-8° are dominated by erosion, while the distal reach (5°-2°) erosion and deposition processes act simultaneously. In the distal reach of the ravine, the erosion or deposition processes tends to be promoted preferentially one over the other, also depending upon the channel width between events. Only for extraordinary rainfall events, lahars are mostly erosive all along the ravine up to the distal fan where deposition take place.

These results can be used as a tool to foresee the effects of future laharic events in Volcán de Colima, and as a tool to improve the input parameters for the modelling of these flows along other volcanoes (e.g., the Popocatépetl volcano, see Caballero and Capra, 2014), in order to determine the hazard zonation for lahars in this volcano.

The 2013-2014 period was characterized by a very low explosive activity at Volcán de Colima, during which only small rock falls and pyroclastic flows formed at the beginning of the 2013 and at the end of 2014. As previously observed (Capra et al., 2010) lahar frequency increases right after an eruptive phase and decreases during the following years, but this study evidences that the number of the events is not directly related with the erosion/depositional rate, as the amount and intensity of rainfall still remains the main factor in controlling flow discharge (magnitude) and duration. The volcano landscape recovered its hydrological and sediment-yield equilibrium in less than five years and that only largest and long-lasting lahars can catastrophically modify the ravine morphology.

A series of BAFs that occurred during the dome collapse episode of 10-11 July 2015 at Volcán de Colima dramatically changed the morphology of Montegrande ravine, filling up the main channel up to its distal fan (Capra et al., 2016), and became rectilinear altering its geomorphic and hydrological features again. These new geomorphic conditions will probably lead to the formation of a new morphology and to the change of the characteristics of the flows of the next rainy season that will likely involve large amount of sediment.

Acknowledgments

This work was supported by CONACyT 99486, PAPIIT-UNAM IN-106710, SRE-CONACyT 146324 projects to Lucia Capra. Thanks to the staff of Centro Nacional de Prevención de Desastres (CENAPRED) for the setup of the instrumentation on Montegrande monitoring site. Thanks to Penélope López for managing the Spot image acquisition from ERMEX-SPOT IMAGE S.A. We also thank to all the students and colleagues that helped in taking the topographic profiles during the seasons.

References

Abancó, C. and Hürlimann, M.: Estimate of the debris-flow entrainment using field and topographical data, Nat. Haz., 71(1), 363–383, doi:10.1007/s11069-013-0930-5, 2014.

Andrés de Pablo, N., Zamorano, J.J., and Blasco J.J.S.: Evolución post-lahárica de un canal proglaciar: garganta de Huiloac (México), Bol. Soc. Geol. Mex., 66(2), 305-328, 2014.

Berger, C., McArdell, B.W., and Schlunegger, F.: Direct measurement of channel erosion by debris flows, Illgraben, Switzerland., J. Geophys. Res., 116 (F1), doi: 10.1029/2010JF001722, 2011.

Beverage, J. and Culbertson, J.: Hyperconcentrations of suspended sediment, Am. Soc. Civ. Eng., 90, 117-126, 1964.

Caballero, L. and Capra, L.: The use of FLO2D numerical code in lahar hazard evaluation at Popocatépetl volcano: a 2001 lahar scenario, Nat. Haz. Earth Sys. Sci., 14, 3345-3355, 2014.

Capra, L., Poblete, M.A., and Alvarado, R.: The 1997 and 2001 lahars of Popocatépetl volcano (Central Mexico): textural and sedimentological constraints on their origin and hazards, J. Volcanol. Geotherm. Res., 131, 351-369, 2004.

Capra, L., Borselli, L., Varley, N., Gavilanes-Ruiz, J.C., Norini, G., Sarocchi, D., Caballero, L., and Cortes, A.: Rainfall-triggered lahars at Volcán de Colima, Mexico: Surface hydro-repellency as initiation process, J. Volcanol. Geotherm. Res., 189, 105-117, 2010.

Capra, L., Roverato, M., Gropelli, G., Sulpizio, R., Arámbula-Mendoza, R., Reyes, G., Lube, G., and Cronin, S.J.: Hurricane-triggered lahars at Volcán de Colima: evidences of flow dynamic from monitoring and field survey, Abstract with program IAVCEI, Kagoshima, Japan, 2013.

Capra, L., Gavilanes-Ruiz, J.C., Bonasia, R., Saucedo-Giron, R., and Sulpizio, R.: Re-assessing volcanic hazard zonation of Volcán de Colima, México, Nat Haz., 76, 41-61, doi: 10.1007/s11069-014-1480-1, 2015.

Capra, L., Macías, J.L., Cortés, A., Dávila, N., Saucedo, R., Osorio-Campo, S., Arce, J.L., Gavilanes-Ruiz, J.C., Corona-Chávez, P., García-Sánchez, L., Sosa-Ceballos, G., and Vázquez, R.: Preliminary report on the July 10-11, 2015 eruption at Volcán de Colima: Pyroclastic density currents with exceptional runouts and volume, J. Vol. Geotherm. Res., 310, 39-49, 2016.

Chen, J., He, Y.P., and Wei, F.Q.: Debris flow erosion and deposition in Jiangjia Gully, Yunnan, China, Environ. Geol., 48, 771-777, doi: 10.1007/s00254-005-0017-z, 2005.

Costa, J.E., 1984. Physical geomorphology of debris flows. In: Costa, J.E., Fleisher, P.J. (Eds.), Developments and Applications of Geomorphology, Springer, Berlin, pp. 268-317, 1984.

Costa, J.E.: Rheologic, geomorphic, and sedimentalogic differentiation of water floods, hyperconcentrated flows and debris flows, in: Flood geomorphology, edited by Baker et al., John Wiley and Sons, New York, pp. 113-122, 1987.

Coe, J. A., Kinner, D. A., and Godt, J.W.: Initiation conditions for debris flows generated by runoff at Chalk Cliffs, central Colorado, Geomorphol., 96(3-4), 270–297, doi:10.1016/j.geomorph.2007.03.017, 2008.

Cronin, S.J., Neall, V.E., Lecointre, J.A., and Palmer, A.S.: Dynamic interactions between lahars and streamflow: A case study from Ruapehu volcano, New Zealand, Geol. Soc. Am. Bull., 111, pp. 28-38, doi: 10.1130/0016-7606(1999)111<0028:DIBLAS>2.3.CO;2, 1999.

Davila, N., Capra, L., Gavilanes-Ruiz, J.C., Varley, N., Norini, G., and Gómez-Vazquez, A.: Recent lahars at Volcán de Colima (Mexico): Drainage variation and spectral classification, J. Volcanol. Geotherm. Res., 165, 127-141, 2007.

Doyle, E.E., Cronin, S.J., and Thouret, J-C.: Defining conditions for bulking and debulking in lahars, Geol. Soc. Am. Bull., 123(7-8), 1234-1246, 2011.

Fagents, S.A. and Baloga, S.M.: Toward and model for the bulking and debulking of lahars, J. Volcanol. Geotherm. Res., 111, B10201, doi: 10.1029/2005JB003986, 2006.

Guthrie, R.H., Hockin, A., Colquhoun, L., Nagy, T., Evans, S.G., and Ayles, C.: An examination of controls on debris flow mobility: Evidence from coastal British Columbia, Geomorphol., 114, 601-613, 2010.

Hungr, O., McDougall, S., and Bovis, M.: Entrainment of material by debris flows, in: Debris-flow hazards and related phenomena, edited by Jakob and Hungr, Springer, Berlín Heidelberg, 135-158, 2005.

Iverson, R.M., Reid, M.E., Logan, M., LaHusen, R.G., Godt, J.W., and Griswold, J.P.: Positive feedback and momentum growth during debris-flow entrainment of wet bed sediment, Nat. Geosci., 4(2), 116–121, doi:10.1038/ngeo1040, 2011.

Lavigne, F.: Evolution géomorphologique de la vallée Boyong à la suite de l'éruption du 22 novembre 1994 du volcán Merapi, Java, Indonésie, Géomorphologie Suppl., 46, 123-142, 2001.

Lavigne, F.: Rate of sediment yield following small-scale volcanic eruptions: A quantitative assessment at the Merapi and Semeru stratovolcanoes, Java, Indonesia, Earth Surf. Process. Landforms, 29, 1045-1058, 2004.

Macías, J.L., Saucedo, R., Gavilanes, J.C., Varley, N., Velasco-García, S., Bursik, M., Vargas-Gutiérrez, V., and Cortés, A.: Flujos piroclásticos asociados a la actividad explosiva del Volcán de Colima y perspectivas futuras, GEOS, 25(3), 340-351, 2006.

Major, J.J., Pierson, T.C., Dinehart, R.L., and Costa, J.E.: Sediment yield following severe volcanic disturbance: a two-decade perspective from Mount St. Helens, Geol., 28, 819-822, 2000.

Mangeney, A., Roche, O., Hungr, O., Mangold, N., Faccanoni, G., and Lucas, A.: Erosion and mobility in granular collapse over sloping beds, J. Geophys. Res. Earth Surf., 115(3), 1–21, doi:10.1029/2009JF001462, 2010.

Manville, V., Németh, K., and Kano, K.: Source to sink: A review of three decades of progress in the understanding of volcaniclastic processes, deposits and hazards, Sed. Geol., 220, 136-161, 2009.

McCoy, S. W., Kean, J. W., Coe, J. A., Tucker, G. E., Staley, D. M. and Wasklewicz, T. A.: Sediment entrainment by debris flows: In situ measurements from the headwaters of a steep catchment, J. Geophys. Res. Earth Surf., 117(3), 1–25, doi:10.1029/2011JF002278, 2012.

Milliman, J.D. and Syvitski, J.P.: Geomorphic/tectonic control of sediment discharge to the ocean: the importance of small mountainous rivers, J. Geol., 100, 525-544, 1992.

Mizuyama, T. and Kobashi, S.: Sediment yield and topographic change after major volcanic activity, Proceedings of the Exeter Symposium, IAHS Publication, 236, 1996.

Muñoz-Salinas, E., Renschler, C.S., Palacios, D., and Namikawa, L.M.: Updating cannel morphology in digital elevation models: lahar assessment for Tenenepanco-Huiloac Gorge, Popocatépetl volcano, Mexico, Nat Haz., 45, 309-320, 2008.

Muñoz-Salinas, E., Renschler, C.S., and Palacios, D.: A GIS-based method to determine the volume of lahars: Popocatépetl volcano, Mexico, Geomorphol., 111, 61-69, 2009.

O'Brien, J., Julien, P., and Fullerton, W.: Two-dimensional water flood and mudflow simulation, J. Hydraul. Eng.-ASCE, 119, 244-261, 1993.

Okano, K., Suwa, H., and Kanno, T.: Characterization of debris flows by rainstorm condition at a torrent on the Mount Yakedake Volcano, Japan, Geomophol., 136, 88-94, 2012.

Pierson, T.C.: Flow characteristics of large eruption-triggered debris flows at snow-clad volcanoes: Constraints for debris-flow models, J. Volcanol. Geotherm. Res., 66, 183-194, doi: 10.1016/0377-0273(94)00070-W, 1995.

Pierson, T.C.: Hyperconcentrated flow transition process between water flow and debris flow, in: Debris flow hazards and related phenomena, edited by Jakob and Hungr, Springer-Verlag, New York, 159-196, 2005.

Pierson, T.C. and Costa, J.E.: A rheologic classification of subaerial sediment-water flows, Geol. Soc. Am. Rev. Eng. Geol., 7, 1-12, 1987.

Pierson, T.C. and Scott, K.M.: Downstream dilution of a lahar, transition from debris flow to hyperconcentrated streamflow, Water Resour. Res., 21, 1511-152, doi: 10.1029/WR02li010p01511, 1985.

Pierson, T.C., Pringle, P.T., and Cameron, K.A.: Magnitude and timing of downstream channel aggradation and degradation in response to a dome-building eruption at Mt. Hood, Oregon, Geol. Soc. Amer. Bull., 123, 3-20, 2011.

Procter, J., Cronin, S.J., Fuller, I.C., Lube, G., and Manville, V.: Quantifying the geomorphic impacts of a lake-breakout lahar, Mount Ruapehu, New Zealand, Geol., 38(1), 67-70, doi: 10.11307G30129.1, 2010.

Scott, K.M.: Origins, behavior, and sedimentology of lahars and lahar-runout flows in the Toutle-Cowlitz River system, U.S. Geological Survey Professional Paper, 1447-A, 47 p, 1988.

Scott, K.M., Vallance, J.W., Kerle, N., Macias, J.L., Strauch, W., and Devoli, G.: Catastrophic precipitation-triggered lahar at Casita volcano, Nicaragua: Occurrence, bulking, and transformation, Earth Surf. Proc. Land., 30, 59-79, doi: 10.1002/esp.1127, 2005.

Smith, G.A. and Fritz, W.J.: Volcanic influences on terrestrial sedimentation, Geol., 17, 375-376, 1989.

Starheim, C., Gomez, C., Daves, T., Lavigne, F., and Wassmer, P.: In-flow evolution of lahar deposits from video-imagery with implications for post-event deposit interpretation, Mount Semeru, Indonesia, J. Volcanol. Geotherm. Res., 256, 96-104, 2013.

Sulpizio, R., Capra, L., Sarocchi, D., Saucedo, R., Gavilanes-Ruiz, J.C., and Varley, N.R.: Predicting the block-and-ash flow inundation áreas at Volcán de Colima (Colima, Mexico) based on the present day (February 2010) status, J. Volcanol. Geotherm. Res., 193, 49-66, 2010.

Theule, J.I., Liébault, F., Laigle, D., Loye, A., and Jaboyedoff, M.: Channel scour and fill by debris flows and bedload transport, Geomorphol., 243, 92-105, 2015.

Thouret J.C., Oehler, J.F., Gupta, A., Solikhin, A., and Procter, J.N.: Erosion and aggradation on persistenly active volcanoes – a case study from Semeru Volcano, Indonesia, Bull. Volcanol., 76:857, doi 10.1007/s00445-014-0857-z, 2014.

Vallance, J.W.: Lahars, in: Encyclopedia of volcanoes, edited by Sigurdsson et al., Academic Press, New York, 601-616, 2000.

Vázquez, R., Capra, L., Caballero, L., Arámbula-Mendoza, R., and Reyes-Dávila, G.: The anatomy of a lahar: Deciphering the 15th September 2012 lahar at Volcán de Colima, Mexico, J. Volcanol. Geotherm. Res., 272, 126-136, 2014.

Vázquez, R., Suriñach, E., Capra, L., Arámbula-Mendoza, R., Reyes-Dávila, G.: Seismic characterisation of lahars at Volcán de Colima, Mexico, Bull. Volcanol., 78(8), doi: 10.1007/s00445-016-1004-9, 2016.

Walling D.E. and Webb, B.W.: Erosion and sediment yield: a global overview, Proceedings of the Exeter Symposium, IAHS Publication, 236, 3-19, 1996.

Yang, C.T.: Sediment transport, theory and practice, McGraw-Hill, New York, N.Y, 1996.

Zeller, M.E. and Fullerton, W.T.: A theoretically derived sediment transport equation for sand-bed channels in arid regions, Proceedings of the D.B. Simons Symposium on Erosion and Sedimentation, Colorado State University and ASCE, 1983.

Nat. Hazards Earth Syst. Sci. Discuss., doi:10.5194/nhess-2016-138, 2016
Manuscript under review for journal Nat. Hazards Earth Syst. Sci.
Published: 12 May 2016

Natural Hazards and Earth System Sciences
Open Access
Discussions

Table I. Classification and features of the lahars developed during the 2013 and 2014 rainy seasons, along with the first lahar of the 2015 season, on Montegrande ravine.

Event	Duration (hrs)	Accumulated rainfall (mm)	Rainfall intensity (mm/h)	Classification
11 June 2013 (Vázquez et al., 2016)	3	117	131	MPE*
11-12 June 2013 Field campaign				
15 June 2013	2	54.4	112	MPE
24 July 2013 (Vázquez et al., 2016)	1.5	25	56	SPE**
30 July 2013 Field campaign				
16 September 2013 (Triplet lahars)	2, 1.8, 2.5	----	----	MPEs
11 October 2013 Field campaign				
2 July 2014	1.5	----	----	SPE
3 July 2014	1.5	----	----	MPE
4 July 2014	2	7.4	19	SPE
7 July 2014 (The twin lahars)	1.5, 1.5	7.8, 18.6	31.5, 26	MPEs
15 July 2014	2	3.4	6	MPE
6 August 2014	1.5	14	95	MPE
12 September 2014 Field campaign				
17 March 2015	1.5, 1.3	----	----	MPE
18 March 2015 Field campaign				

Nat. Hazards Earth Syst. Sci. Discuss., doi:10.5194/nhess-2016-138, 2016
Manuscript under review for journal Nat. Hazards Earth Syst. Sci.
Published: 12 May 2016

Natural Hazards and Earth System Sciences
Open Access
Discussions

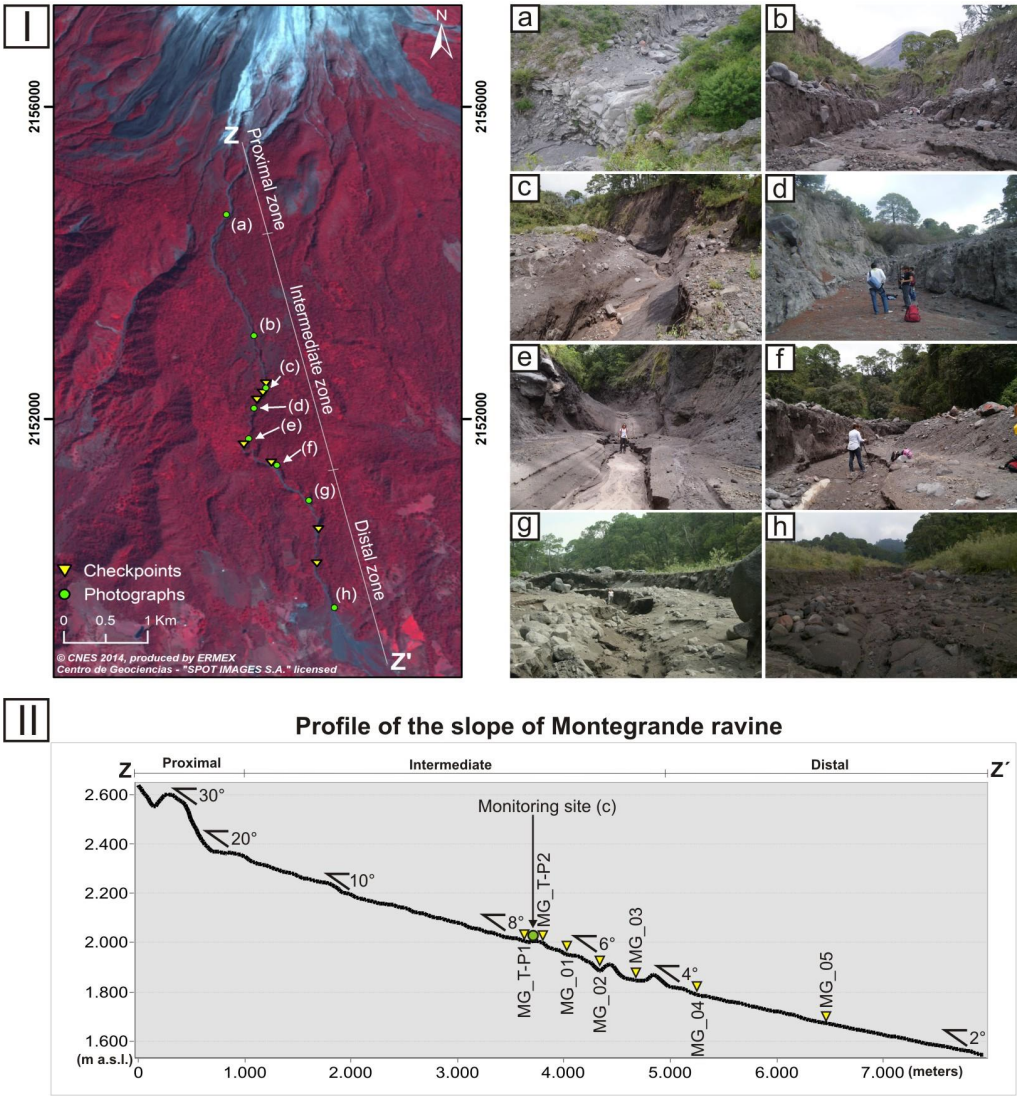

Figure 1: [I] SPOT 5 image (1, 2, 3, and 4 bands in RGB combination, 5 m of resolution) of Volcán de Colima showing the Montegrande ravine and the location of the checkpoints. Yellow triangles represent the location of the analyzed cross-sections, green dots the location where the photos were taken: within the proximal zone (a, and b); the intermediate zone (c, d, e, and f) and at the distal zone (g, and h). [II] Topographic profile along the ravine, showing its slope values, the location of the checkpoints and the monitoring site.

Nat. Hazards Earth Syst. Sci. Discuss., doi:10.5194/nhess-2016-138, 2016
Manuscript under review for journal Nat. Hazards Earth Syst. Sci.
Published: 12 May 2016

Natural Hazards and Earth System Sciences
Open Access
Discussions

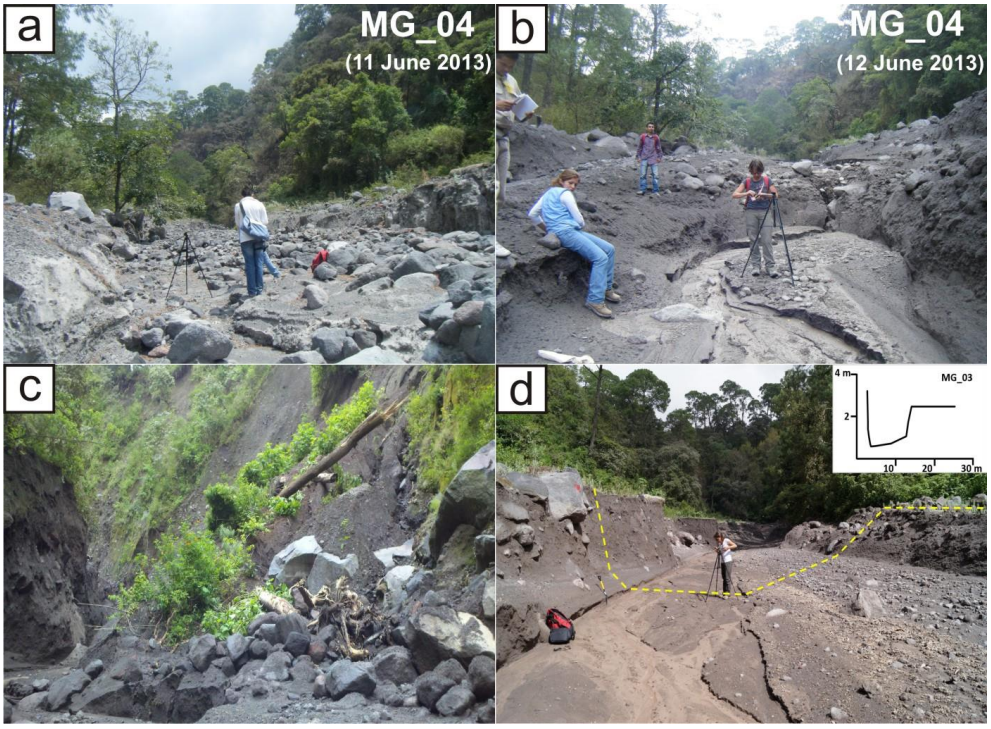

Figure 2: Photographs showing the main morphological features of Montegrande ravine and the changes due the laharic activity. a) Photo of the morphology at MG_04 checkpoint on 11 June 2013 (at the beginning of the rainy season, and before the development of the lahar) b) on 12 June 2013, a day after the lahar, showing the erosion caused by the flow. c) Trees and debris obstructing the main channel of the ravine accumulated during the dry season due to small landslides. d) Photo of one of the checkpoints, with the sketched profile in hatched yellow line and their corresponding measured profile.

Nat. Hazards Earth Syst. Sci. Discuss., doi:10.5194/nhess-2016-138, 2016
Manuscript under review for journal Nat. Hazards Earth Syst. Sci.
Published: 12 May 2016

Natural Hazards and Earth System Sciences
Open Access
Discussions

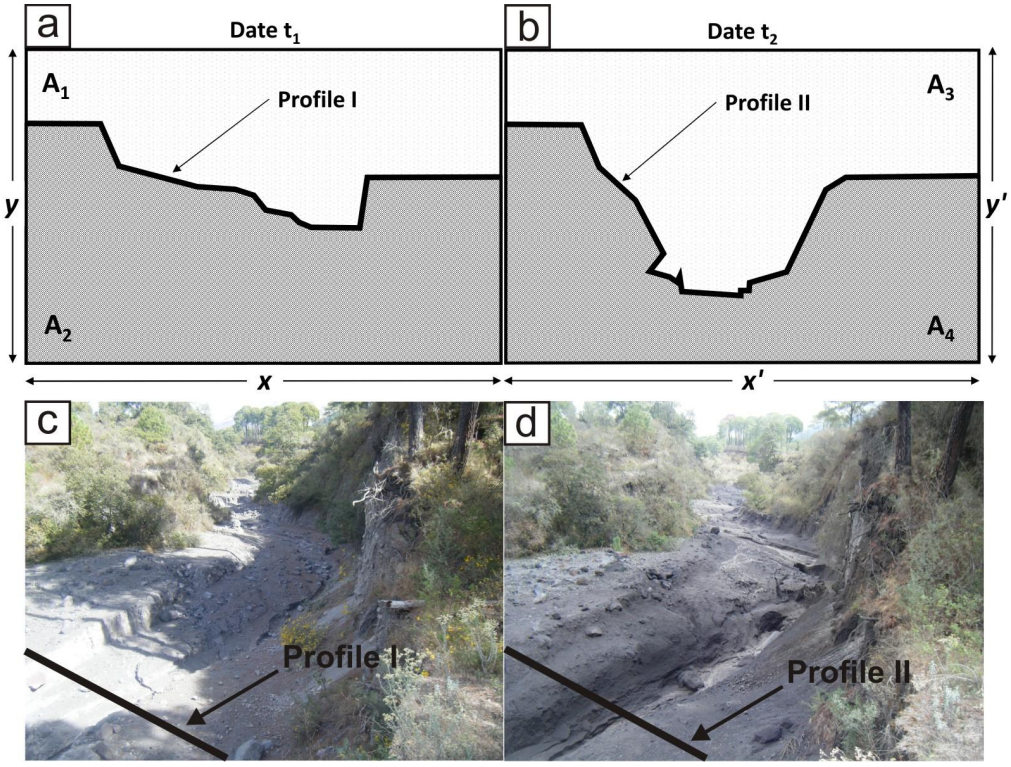

Figure 3: Graphic description of the parameters used in the methodology to determine the E (erosion) and D (deposition) rates within the profiles; and photos taken at the monitoring site of Montegrande ravine, before and after the 11 June 2013 lahar. a) Representation of the topographic profile during Date t_1, and the parameters needed to determine A_T = A1 + A2. b) Representation of the topographic profile changed during Date t_2, and the variation of the parameters needed to determine the areal values. c) Image of the active channel being monitored on 11 June 2013. d) Image of the channel on 12 June 2013.

Nat. Hazards Earth Syst. Sci. Discuss., doi:10.5194/nhess-2016-138, 2016
Manuscript under review for journal Nat. Hazards Earth Syst. Sci.
Published: 12 May 2016

Natural Hazards and Earth System Sciences
Open Access
Discussions

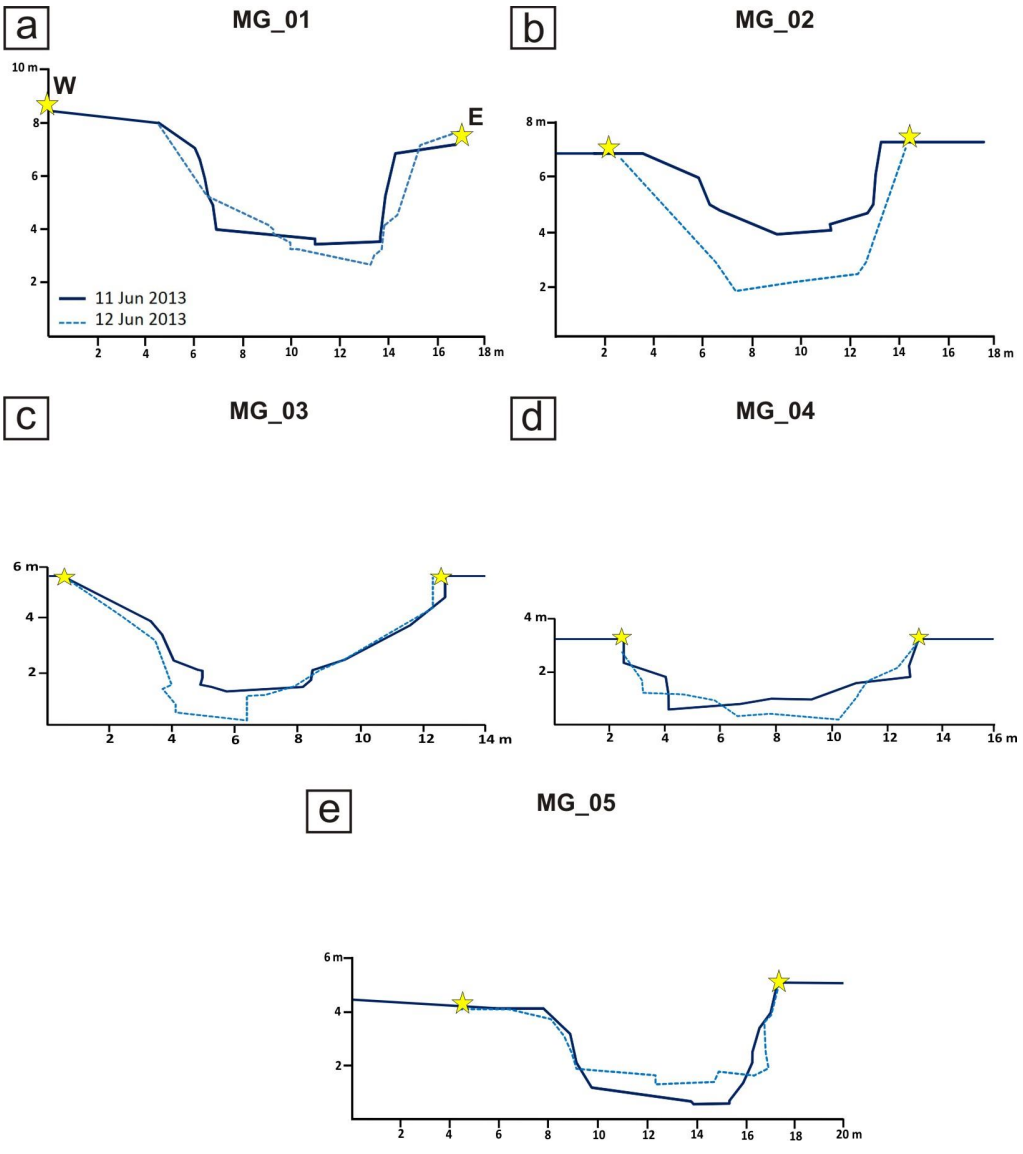

Figure 4: Cross-section profiles before (bold blue lines), and after (hatched lines in light-blue) the 11 June 2013 lahar for the following checkpoints (Fig. 1 for location): a) MG_01. b) MG_02. c) MG_03. d) MG_04. e) MG_05. All the profiles were taken facing up the flow the channel.

Nat. Hazards Earth Syst. Sci. Discuss., doi:10.5194/nhess-2016-138, 2016
Manuscript under review for journal Nat. Hazards Earth Syst. Sci.
Published: 12 May 2016

Natural Hazards and Earth System Sciences
Open Access
Discussions

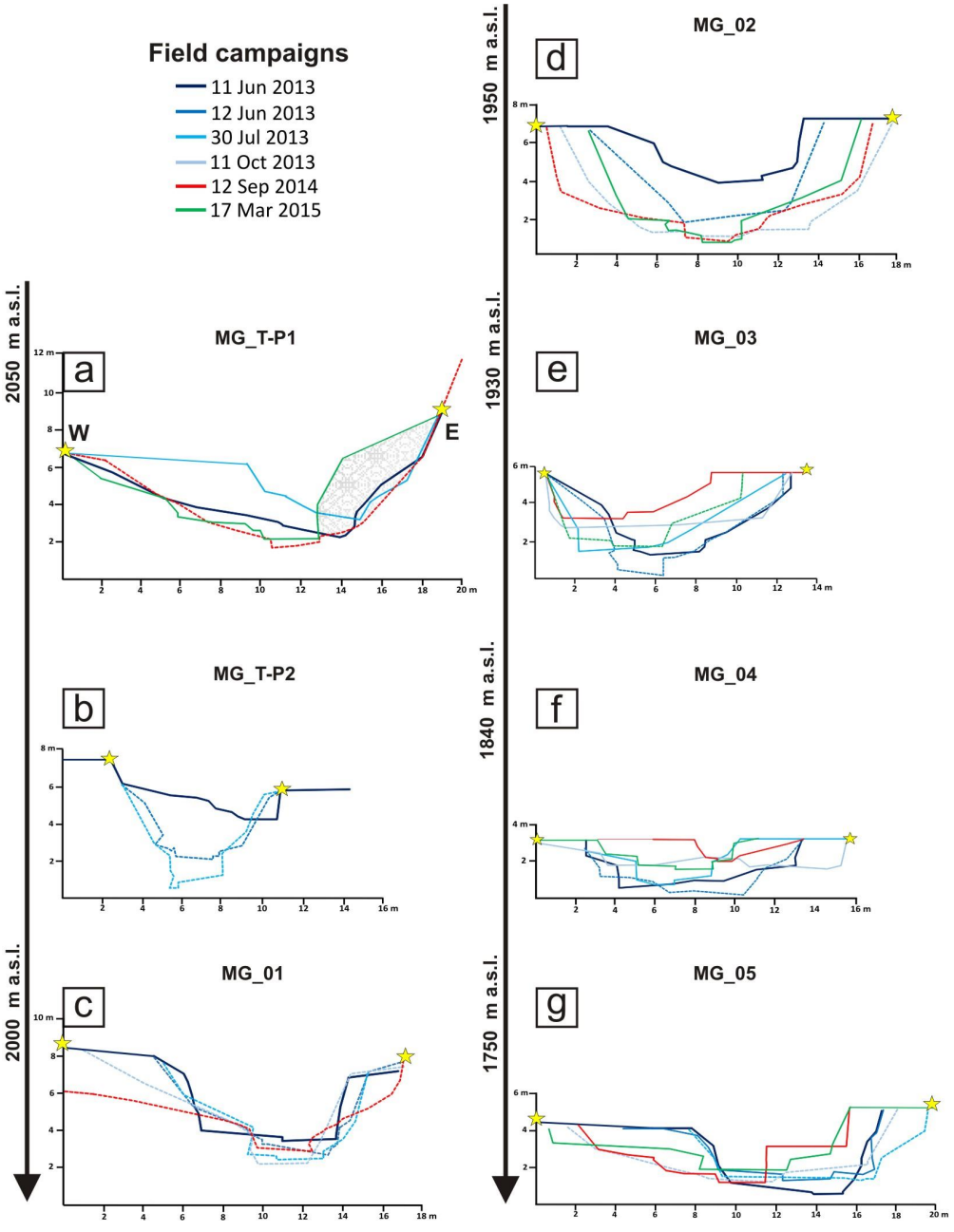

Figure 5: Comparative cross-section profiles of the checkpoints in Montegrande ravine, according to the field campaigns (Fig. 1 for location). a) MG_T-P1. b) MG_T-P2c) MG_01. d) MG_02. e) MG_03. f) MG_04. g) MG_05. The dotted lines represent erosion, and lines represent deposition. The blue colors are related to the 2013 season, while the red and the green lines refers to the 2014 and 2015 season respectively.

Nat. Hazards Earth Syst. Sci. Discuss., doi:10.5194/nhess-2016-138, 2016
Manuscript under review for journal Nat. Hazards Earth Syst. Sci.
Published: 12 May 2016

Natural Hazards and Earth System Sciences
Open Access
Discussions

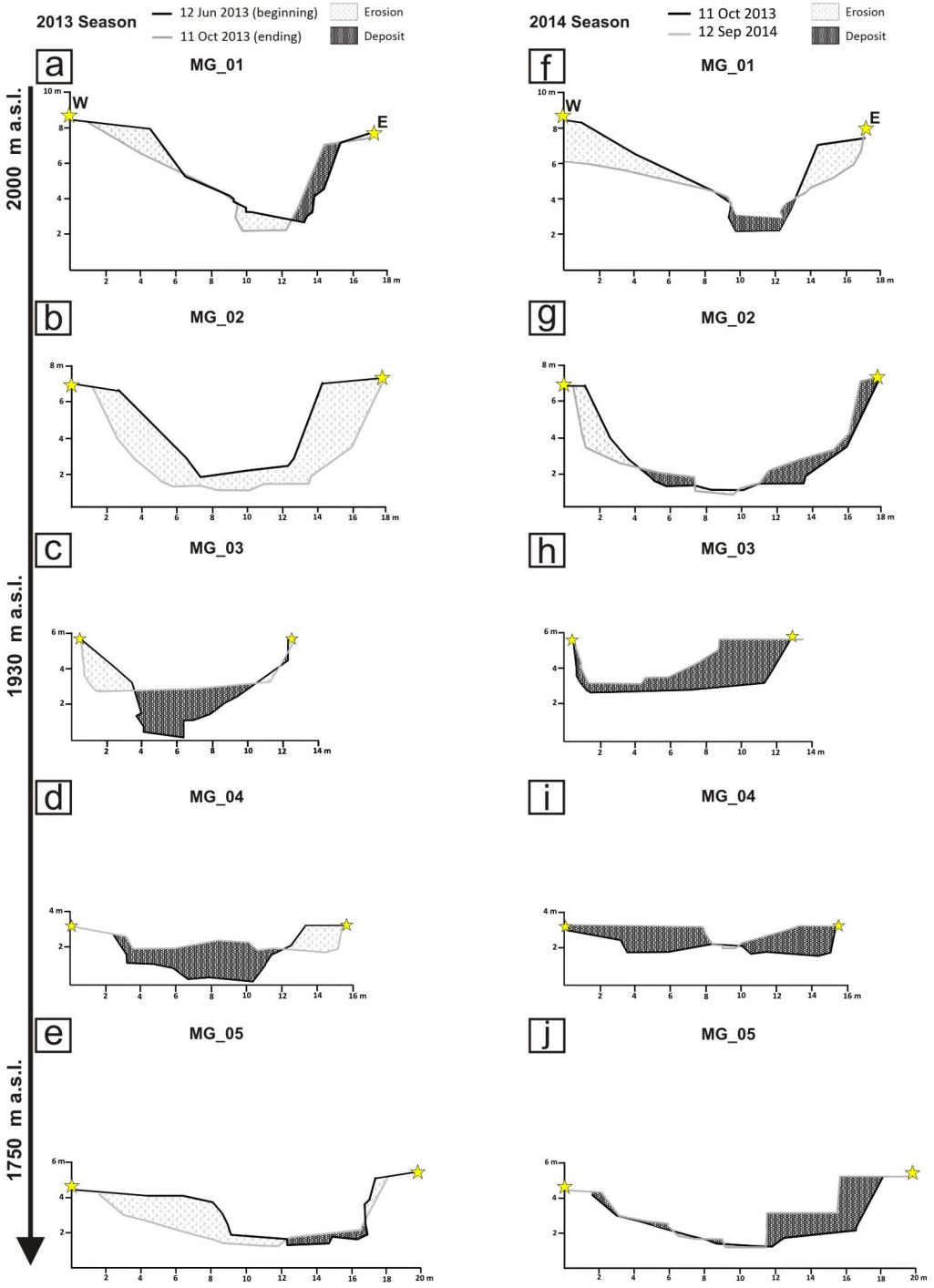

Figure 6: Annual balances during 2013 and 2014 seasons of the erosion-deposition processes from the cross-section profiles of the checkpoints at Montegrande ravine (Fig. 1 for location). For the 2013 season: a) MG_01 b) MG_02.

Nat. Hazards Earth Syst. Sci. Discuss., doi:10.5194/nhess-2016-138, 2016
Manuscript under review for journal Nat. Hazards Earth Syst. Sci.
Published: 12 May 2016

Natural Hazards and Earth System Sciences
Open Access
Discussions

c) MG_03. d) MG_04. e) MG_05. For the 2014 season: f) MG_01. g) MG_02. h) MG_03. i) MG_04. j) MG_05. The light fill-patterns represent the eroded area within the active channel and the darker fill-patterns represent deposition.

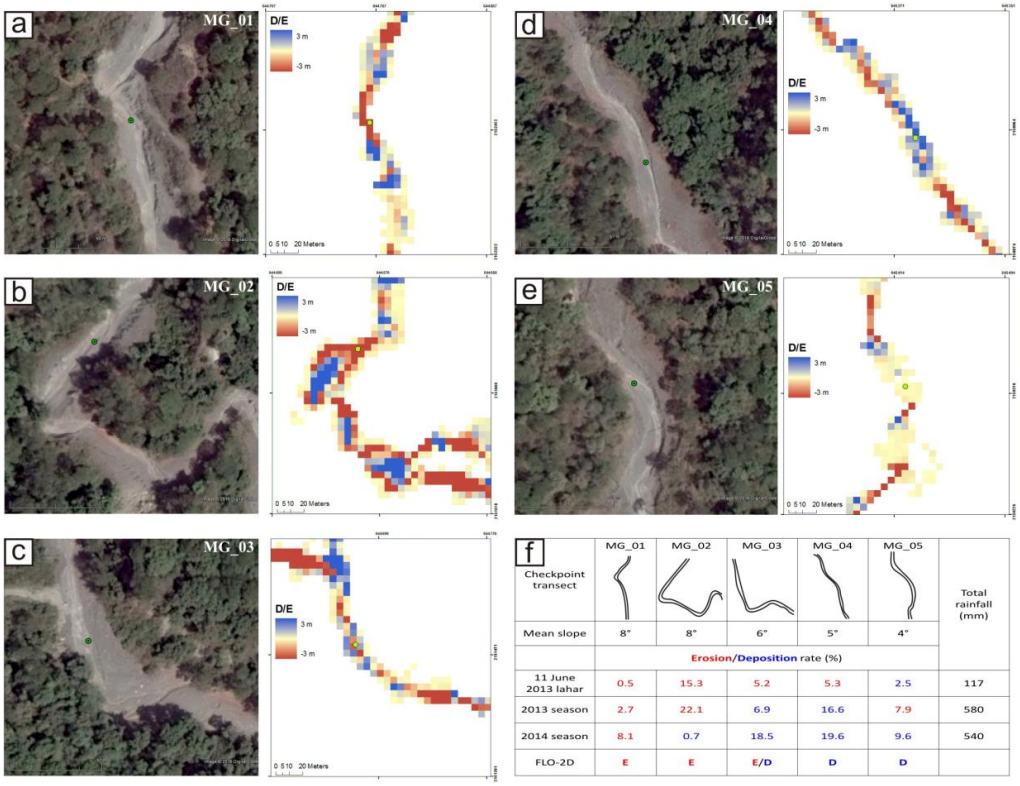

Checkpoint transect	MG_01	MG_02	MG_03	MG_04	MG_05	Total rainfall (mm)
Mean slope	8°	8°	6°	5°	4°	
	Erosion/Deposition rate (%)					
11 June 2013 lahar	0.5	15.3	5.2	5.3	2.5	117
2013 season	2.7	22.1	6.9	16.6	7.9	580
2014 season	8.1	0.7	18.5	19.6	9.6	540
FLO-2D	E	E	E/D	D	D	

Figure 7: Results of the FLO-2D model for the erosion/deposition processes along the Montegrande ravine at each checkpoint. Negative values refer to erosion as positive values refer to deposition. Google images are also presented to better appreciate the morphology at each checkpoint: a) MG_01 b) MG_02 c) MG_03 d) MG_04. e) MG_05. f) Table showing the *D/E* rates obtained from the analysis at the checkpoints for the 11 June 2013 lahar, and the 2013-2014 seasons, compared with the qualitative results obtained from the FLO-2D model. All the images are from Google Earth scenes, from 3rd April 2014. The green dots indicate the exact location where the cross-section profiles were taken.

Nat. Hazards Earth Syst. Sci. Discuss., doi:10.5194/nhess-2016-138, 2016
Manuscript under review for journal Nat. Hazards Earth Syst. Sci.
Published: 12 May 2016

Natural Hazards and Earth System Sciences
Open Access
Discussions

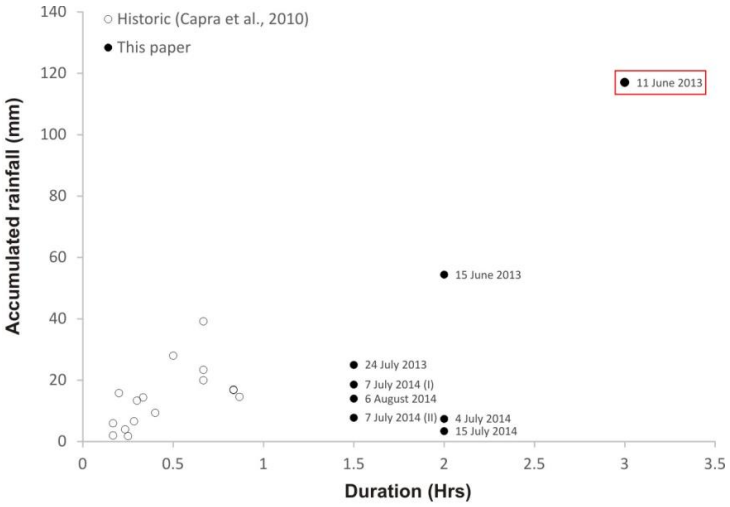

Figure 8: Comparative plot of accumulated rainfall vs. duration of historic and recent events that triggered lahars at Volcán de Colima. The historical data, represented with empty dots were taken from Capra et al. (2010), and are from 2007-2009 years. The black dots represent the data from this paper, and the extraordinary event of 11 June 2013 is signaled with a red box.

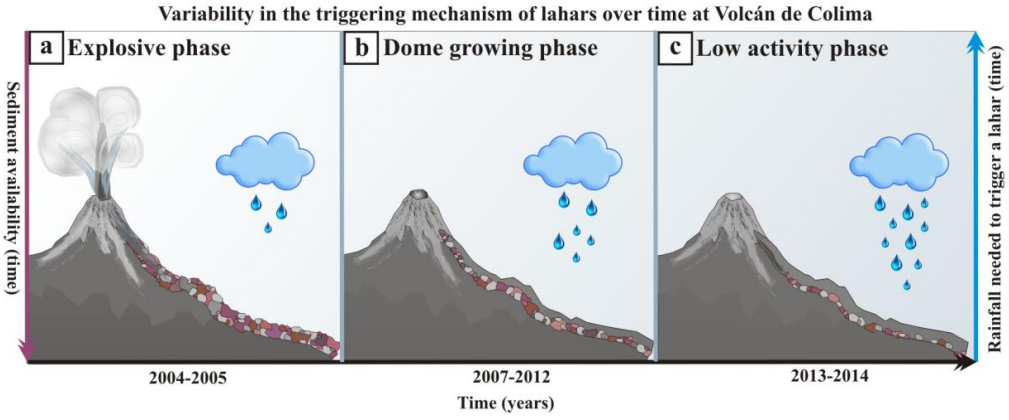

Figure 9: Conceptual model of the variability in the conditions needed to trigger a lahar over time at Volcán de Colima. a) After the main explosive phase during 2004-2005, the slopes of the volcano were filled with material, and the rate of rainfall needed to trigger a lahar was minor. b) During the dome growing phase (from 2007-2012), the amount of material decreased, while the amount of rainfall needed to trigger lahars were increasing over time. c) Finally, during the phase of lowest eruptive activity (from 2012-2015), the rate of material available to form lahars was diminishing, while a major quantity of rainfall was needed to trigger the flows.